Performance Evaluation of a Small-Scale Magnetorheological damper for Civil Engineering Applications

Shamurailatpam Vivekananda Sharma[1], Hemalatha Gladston[1] and Arunraj Ebanezer[1]

[1] *Karunya Institute of Technology and Sciences, Department of Civil Engineering, 641114, Coimbatore, India*

Corresponding author:
Shamurailatpam Vivekananda Sharma
bom03vivek@gmail.com

Abstract:
Magnetorheological dampers (MRDs) are devices that adjust their damping properties in response to an external magnetic field. Large-scale MRDs have been successfully used as vibration control devices in structures. This study focuses on modelling and optimizing an MRD using COMSOL Multiphysics. Various parameters, such as coil turns and current, are optimized to achieve the maximum flux value in the MRD. The simulation yielded a maximum magnetic flux of 0,44 T with 500 coil turns. Based on the optimized MRD parameters, a numerical equation is then used to calculate the total damping force. The maximum numerical and experimental damping forces corresponding to a 2,0 A current were 989,39 and 1004,63 N, respectively. The numerical damping force is then compared to the experimental results to validate the accuracy of the model. The MRD is integrated into a scaled-down reinforced concrete frame and subjected to a cyclic loading test for performance evaluation. The results show that the MR dampers improve the performance of the frame structure, increasing its load-carrying capacity and energy dissipation by 19,45 % and 20,43 %, respectively. The findings of the study provide valuable insights into the behaviour of MRDs and their optimization using numerical simulations, as well as highlight the importance of experimental validation for accurate prediction of the performance of MRDs in practical civil engineering applications.

Keywords:
magnetostatic analysis; force-displacement; force-velocity; damping force; energy dissipation

1   Introduction

Civil engineering has traditionally emphasized research on the dynamic responses of structures subjected to various loading conditions [1]. Vibrations caused by earthquakes, wind forces, and other dynamic loads can result in damage to the structure, poor performance of the building, and risk to the safety of the occupants. To address these challenges, engineers have been investigating new technological developments to improve the robustness and responsiveness of civil engineering structures. MRDs are an example of such a technology that has garnered significant attention [2, 3]. MR dampers are innovative semi-active control devices that adaptively adjust damping characteristics based on real-time structural response. This ability allows MR dampers to be used in a variety of applications. Structural engineering has been revolutionized by these dampers, which efficiently mitigate vibrations and improve structural performance [4-7]. These dampers were developed by applying smart materials and sophisticated control systems. MR dampers have become widespread in the construction of civil engineering structures, such as high-rise buildings, bridges, and other essential pieces of infrastructure. By integrating MR dampers into the design of new structures or the retrofitting of existing ones, engineers can significantly improve the capacity of these structures to withstand and mitigate the effects of vibrations and seismic forces. Because of the adjustable damping characteristics of MR dampers, structures can adapt to various dynamic loads, resulting in a solution that is both flexible and responsive [8-14].

Rabinow [15] discovered Magnetorheological Fluids (MRFs), which were typically used in dampers to generate a tuneable damping coefficient. A typical MRF is a suspension of micron-sized magnetic particles in a suitable carrier medium, such as mineral or synthetic oil, which changes its mechanical properties, viscosity, and stiffness when exposed to electric currents or magnetic fields [16]. An MRF can also contain additives (stabilizers and surfactants) that aid particle suspension stability and improve rheological properties. When a liquid is confined between a piston and an inner cylinder with a gap range of 0,5 to 2 mm, chains of particles oriented perpendicular to the Magnetic Flux (MF) direction obstruct fluid movement, thus increasing viscosity [17].

Unlike fully active control systems, MRDs are semi-active control devices that can also be powered by batteries. The performance of an MRD is affected by the MF saturation and the shear yield delivered by the electromagnet. MRDs have been used as vibration control devices in various engineering domains MRDs can also potentially provide a significant damping force (DF) in practical applications such as vehicle suspension and landing gear [18]. They can be used as a vibration control system in railway bridges, heavy structures prone to vibration, and seismic excitation on a larger scale [19]. Biswal and Rao [20] created a 2D axisymmetric model of an MRD using ANSYS FE to simulate the magnetic field distribution for an induced current. Gurubasavaraju et al. [21] used ANSYS to perform magnetostatic analyses on three piston heads made of different materials to calculate the DF of the damper. The MF strength is proportional to the damping force of the MRD. Purandare et al. [22] employed FEM COMSOL for magnetostatic simulation. Using MC theory, they verified the flux density, intensity, and yield stress of an MRF using the FE model. Li and Yang [23] created a numerical model that predicts the MRD's damping force. The mechanical properties of MRFs were characterized using the Bingham model, and the mechanical behaviour of the MRD was investigated under varying currents and excitations. The yield stress of the MRF was determined using Ansoft Maxwell 14.0. The results were utilized to investigate how the MRD worked. Liu et al. [24] created a novel MRD with folding resistance gaps and a bending MC to improve damping performance. By structuring the multi-stage folded annular gap structure, they expanded the length of the resistance gap and developed an MC to activate the no-flux zone. Elsaady et al. [25] used an original one-way coupled numerical technique to predict the dynamic behaviour of the twin-tube MRD. They found that fluid compressibility has a crucial impact on the hysteretic behaviour of the twin tube MRD. The results show that non-Newtonian viscosity is higher in the throttling area, and Newtonian viscosity is lower elsewhere. Furthermore, they demonstrated that changing damper design factors, such as magnetic pole width, input

current, and piston motion frequency, considerably affect damper behaviour. Ganesha et al. [26] studied the magnetic field enhancement method using a single cylindrical shield and a cylindrical sandwich shield integrated into a twin-tube single-coil MRD. The MRD arrangement with a copper alloy shield shows a significant overall improvement in the magnetic field strength.

Gurubasavaraju et al. [27] compared experimental and computational methods to evaluate a twin-tube MRD and provided a computational alternative to experimental testing during the basic design stage. They initially characterized MRDs at 1,5 and 2,0 Hz for stroke lengths of 5 mm and DC currents of 0,1 to 0,4 A. Under the same experimental conditions, they determined the DF using a coupled FEA and CFD analysis. They also used this computational approach to compute and display the DF at 1,5; 2,0; 3,0 and 4,0 Hz. The study showed computational results that agree with the conclusion that the DF is inversely proportional to the fluid flow gap. Cheng et al. [28] proposed an MRD using a meandering MC to improve DF performance. The MRD with a meandering magnetic circuit concept (MMCMRD) uses magnetic and nonmagnetic components to direct the MF. The MMCMRD increases the efficiency of the MRD, and the theoretical model accurately characterizes its DF performance. Aziz et al. [29] used CFD and FE to model the dynamics and DF of a shear-mode MRD. They determined the magnetic field-dependent shear stress of MRP60 based on the relationship between shear stress and magnetic strength.

Shiao et al. [30] developed an adaptable valve for a train with an MRF control system. According to the modelling results, the temperature of the MRF increased but did not exceed operating limits. Hu et al. [31] created a volume-limited geometrically optimized MR valve. They combined the Taguchi orthogonal experiment and response surface methodology with a COMSOL FE model (FEM) for the optimization process. The DF of the MR valve-controlled cylinder system increased by 46 % at 1,25 A, from 2,50 to 3,65 kN, demonstrating RSM and optimal design. To examine the dynamic behaviour of multi-coil MRDs from micro to macro perspective, Yang et al. [32] designed and tested a three-coil MRD. They evaluated the performance of the three-coil MRD for varying currents, amplitudes, frequency ranges, and coil configurations.

Gurubasavaraju [33] proposed modelling a double damper and evaluating its dynamic behaviour with ANSYS. They used FE analysis for electro-MC analysis and design. They computed the MF induced in the fluid region at various currents.

The COMSOL software for engineers and scientists simulates interactions across all disciplines (heat transfer, vibration, fluid dynamics, structural dynamics, physics, electromagnetic response, magnetostatic concerns, etc.). It also provides users access to nearly every engineering simulation discipline required throughout any design process, such as structural analysis. Designers can also use its pre-processing capabilities to create geometry. Once the boundary conditions have been defined and the analysis has been completed, results obtained in COMSOL can be displayed in either numeric or visual representation. Vivekananda et al. [34] presented the FE study of an indigenously built, small-scale MRD. They determined the MF via the FE model to understand the effect of MF inside the damper.

The literature presents works based on a numerical/analytical approach, but most of them are not validated against experimental data. To fabricate a desired MRD for incorporation in civil engineering structure as a vibration control device, it is critical to understand the behaviour, performance, and parameters governing the performance of the MR damper since the device is aimed to dissipate the energy exerted on the structure by external sources. The discussed literature focused on the development and testing of MR damper but was limited to application. This study analyses a small-scale MRD using COMSOL Multiphysics to model and optimize its parameters. Specifically, it optimizes coil turns and current to obtain the maximum flux value that directly impacts the MRD's performance. Finally, it incorporates the developed MRD into a 1:3 scaled-down reinforced concrete frame to study the frame's ultimate load-carrying capacity subjected to a cyclic loading test.

2 Analytical approach

2.1 3D and magnetostatic models of MRD

The appropriate range of DF is a critical consideration when designing an MRD. Therefore, materials for various components of the MRD, such as the cylinder, piston, MRF, and piston rod, are chosen. The DF of the damper depends on the magnetic field; for this, the MC should have effective electromagnetic behaviour to function correctly. The cylinder and piston should be made of soft metals for increased magnetizability. A thorough literature analysis shows that low-carbon steel (SA-1018) is an excellent option for magnetic performance because of its low carbon content [35, 36].
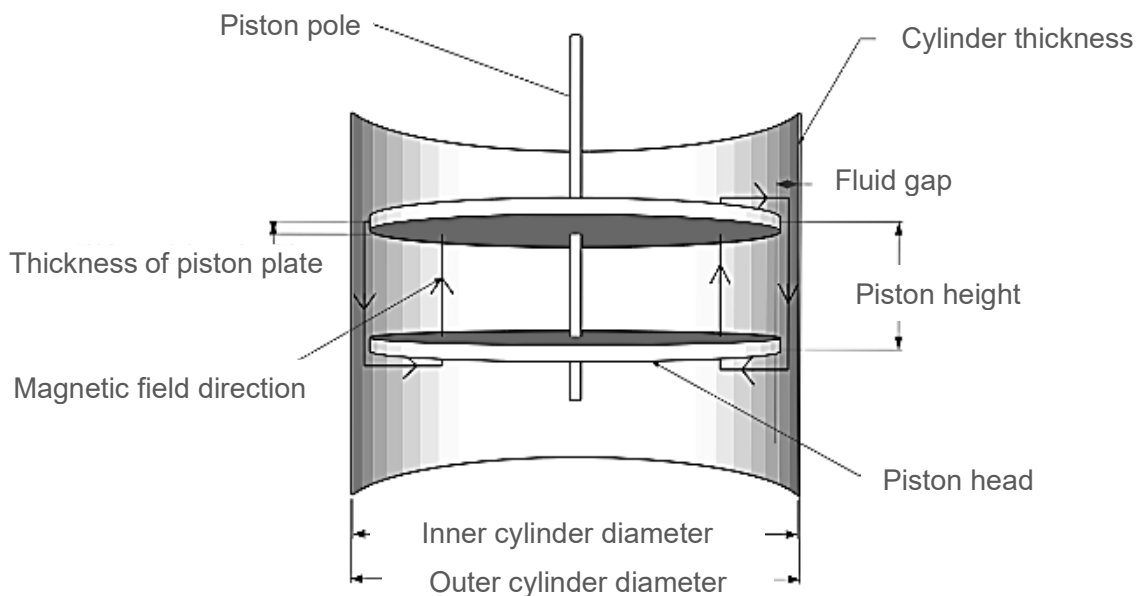

Figure 1. Components of the MRD

**Table 1. Geometric properties used in the MRD model [34]**

Parameters	Dimensions (mm)
Inner diameter of cylinder	40
Outer diameter of cylinder	44
Cylinder thickness	2
Annular gap	1
Piston head	38
Piston height	10
Thickness of piston plate	5

Figure 1 illustrates the schematic of the MC (magnetic circuit) loop in the proposed MRD, while Table 1 presents the dimensions of the prototype MRD used in the design. Figure 2 presents the 3D model of the MRD created in SolidWorks. The model comprises individual parts such as the cylinder, piston rod, piston head, and top cap, which are designed separately and then assembled to form the entire model.
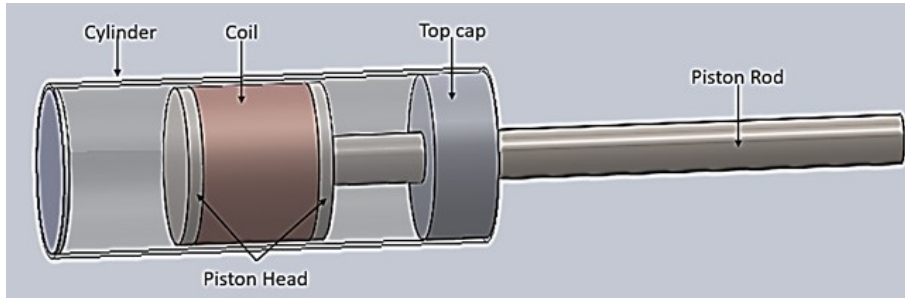
Figure 2. 3D model of MRD in Solid Works

The magnetic field created in the working fluid clearance region mainly determines the DF generated by the MRD. A 3D FEM (Magnetostatic) model is built and analysed [34]. Figure 3 shows the meshed model after material attribution. Figure 4 presents the procedure employed in COMSOL for a magnetostatic analysis of the MRD [37].
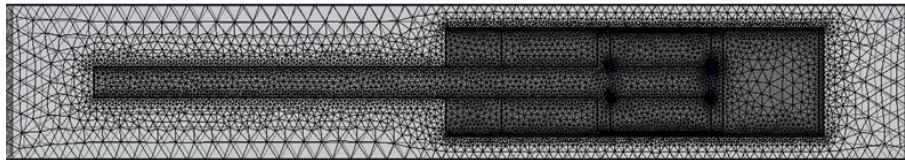
Figure 3. Extra-fine meshing used in the model of the developed small-scaled MRD

Many researchers have expressed an interest in this area and have conducted their investigations using the FE Method (FEM), which is used to model and design MRD [38, 39]. They examined its modelling from various design perspectives. This research has led to the development of numerous MRDs with different configurations, practical DF ranges, and operating principles. When designing the damper and calculating the pressure gradient of the flow through it, the quasi-static laminar flow of the MR-fluid is assumed to exist inside the damper. The magnetostatic analysis can identify the saturation phenomena in an MC.

The magnetic field created in the working fluid clearance region mainly determines the DF generated by the MRD. A 3D FEM (Magnetostatic) model is built and analysed [34]. Figure 3 shows the meshed model after material attribution. Figure 4 presents the procedure employed in COMSOL for a magnetostatic analysis of the MRD [37].
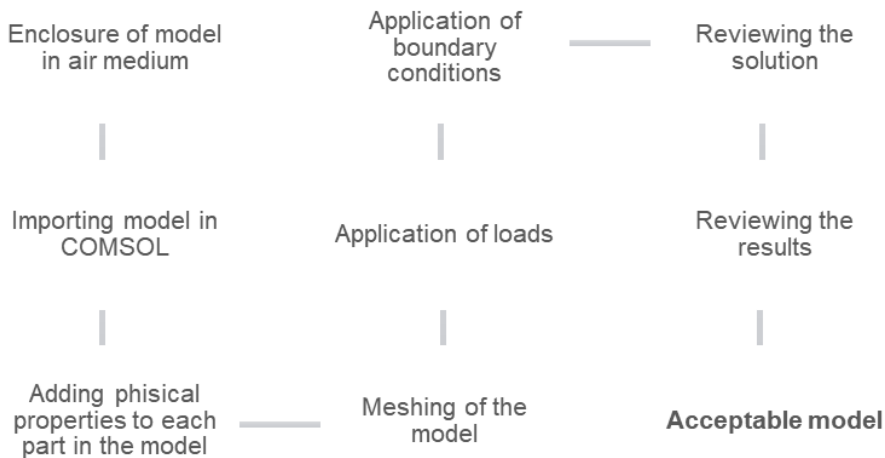
Figure 4. Procedure for magnetostatic analysis of MRD

It is necessary to make assumptions when generating a 3D model [40]. The following assumptions were made for this study:

- o The model is enclosed in an air medium for MF generation.
- o For the element to be visible, it must be located in the global XY, YZ, and XZ planes.
- o Only the element considered in the model can generate magnetic and electric fields.
- o This component cannot achieve structural, thermal, or piezoelectric effects.
- o Materials with only magnetic and electric characteristics (μo and μx) are used in the analysis.

Except for the piston and MRF in the clearance area, which are both stationary components, all MR components are considered stationary. In 3D modelling, a variable coil turns electromagnetic coil such as 100, 200, 300, 400, and 500-turn electromagnetic coil modelled as a uniform portion represents the electromagnetic field for computing the MF density. The electrical current flowing through the coil must be varied to obtain the corresponding value of the MF density. It is ensured that the piston and cylinder materials are made of cast iron with a relative permeability of 5000 and that the electromagnetic coil has a relative permeability of 1. The relative permeability of MRF is also considered as 1. Calculations in this study started with the magnetic permeability of space (μo) value of 4 x 10-7 H/m [41].

2.2   Physics involved in the simulation

The simulations were run with the COMSOL Multiphysics and Electromagnetics physics modules. Maxwell's equations adopted in COMSOL Manual [37] built a time-dependent solver based on the relationships given as the continuity equation for constant electric charge density:

$$\nabla \cdot J = 0 \tag{1}$$

Ampere's law:

$$\nabla \times \mathrm{H} = J \tag{2}$$

Where H denotes magnetic field intensity and J current density.
MF density and magnetic field intensity are related by:

$$B = \mu_0 \mu_r H \tag{3}$$

Similarly, the relation between current density and electric field intensity is:

$$J = \sigma E + J_e \tag{4}$$

According to these equations, μ_0 and μ_r correspond to the material permeability and σ to the electrical conductivity of the material. The two potentials are derived from Gauss's law:

$$E = -\nabla V \tag{5}$$

and Faraday's law:

$$B = -\nabla A \tag{6}$$

Where V denotes electric scalar potential and A magnetic vector potential.
Finally, using COMSOL's Multi-Turn Coil Domain interface, the J term from Equation 4 was calculated, with the value indicating the impact of the electromagnetic coil on the current density in the air:

$$J_e = \frac{N_{coil} I_{coil}}{A} \emptyset \tag{7}$$

Where N denotes the number of turns of the electromagnetic coil in the piston and I_{coil} applied current.

2.3   Total DF

The DF of the magnetostatic model is estimated based on its magnetic field strength, determined at different current levels. Figure 5 shows the relationship between the yield shear stress (y) and the MF density (B) for the 132DG MRF manufactured by Lord Corporation [41]. Based on Figure 5, the yield shear stress for the MF densities is estimated from the magnetostatic analysis in the previous section and presented in Table 2.

The total DF can be calculated by substituting this value into the following formulae. Equation 2 states that yield stress and MF density are related:

$$\tau_y = (6{,}9 \cdot 10^2) + (4 \cdot 10^4)\beta - (1 \cdot 10^5)\beta^2 + (9{,}1 \cdot 10^4)\beta^3 \tag{8}$$
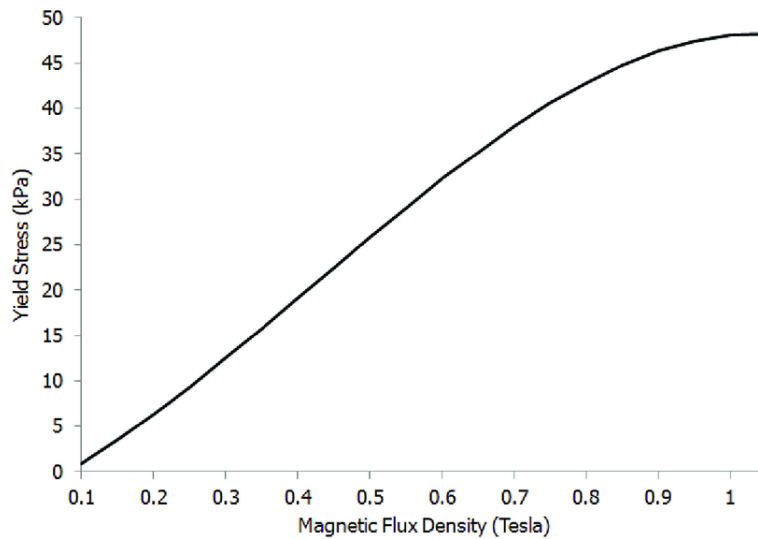
Figure 5. Relationship between yield stress and MF density [34, 40]

According to the Bingham plastic model developed by the plate model [42, 43], the DF, F_D, is a sum of forces induced by yield stress F_τ and F_η as viscous components, i.e.:

$$F_D = F_\tau + F_\eta$$

$$F_D = \left[\left(2{,}07 + \frac{12Q\eta}{12Q\eta + 0{,}4\omega h^2 \tau_y}\right) \cdot \frac{\tau_y L A_p}{h} Sgm(v)\right] + \left[\left(1 + \frac{\omega h v}{2Q}\right) \cdot \frac{12Q\eta L_t A_p}{\omega h^3}\right] \tag{9}$$

where $Q = A_p \cdot v$ is rate of volumetric flow, $A_p = \pi/4(D^2 - d_o^2)$ = C/S area of the piston, D is piston diameter; d_0 piston rod diameter, v piston velocity, τ_y yield shear strength of the MRF, η off-state viscosity of the MRF (no magnetic field), L effective axial pole length, h annular gap, L_t total axial pole length, ω mean circumference of the annular flow path of the damper, and $Sgm(v)$ reciprocating motion of the piston.

MR devices generate some frictional force (F_f) during operation and considered negligible. According to the literature [40, 42, 43]. Thus, DF is the sum of F_τ, F_η and F_f, denoted by the symbol F_D:

$$F_D = F_\tau + F_\eta + F_f \tag{10}$$

Where F_τ denotes force due to yield stress, F_η force due to the viscous component, and F_f force due to friction.

The total DF in the MRD model is then calculated using Equation 10 and is tabulated in Table 2.

3   Experimental validation of the MRD model

3.1   Testing setup

The MTS servo-hydraulic system shown in Figure 6 consists of a load cell, an accumulator, an actuator, a 3000-psi hydraulic power unit, a PC system loaded with MTS Suite software for system control, and a Data acquisition system (Flextest-40) system for real-time data collection. The actuator can generate a dynamic peak force of 1000 kN via the accumulator through the power unit in the frequency range of 0,1 to 2,0 Hz. The actuator's maximum stroke length/amplitude, which can be manually or remotely regulated via the PC system, is ±127 mm. The MTS system can perform bending, compression, dynamic testing, fatigue, fatigue and fracture, tension, stiffness, and strength measurements. Several excitation forms are available, such as Sine, True Sine, Triangle, Square, and Static loading, with an accuracy grade of 1 %.
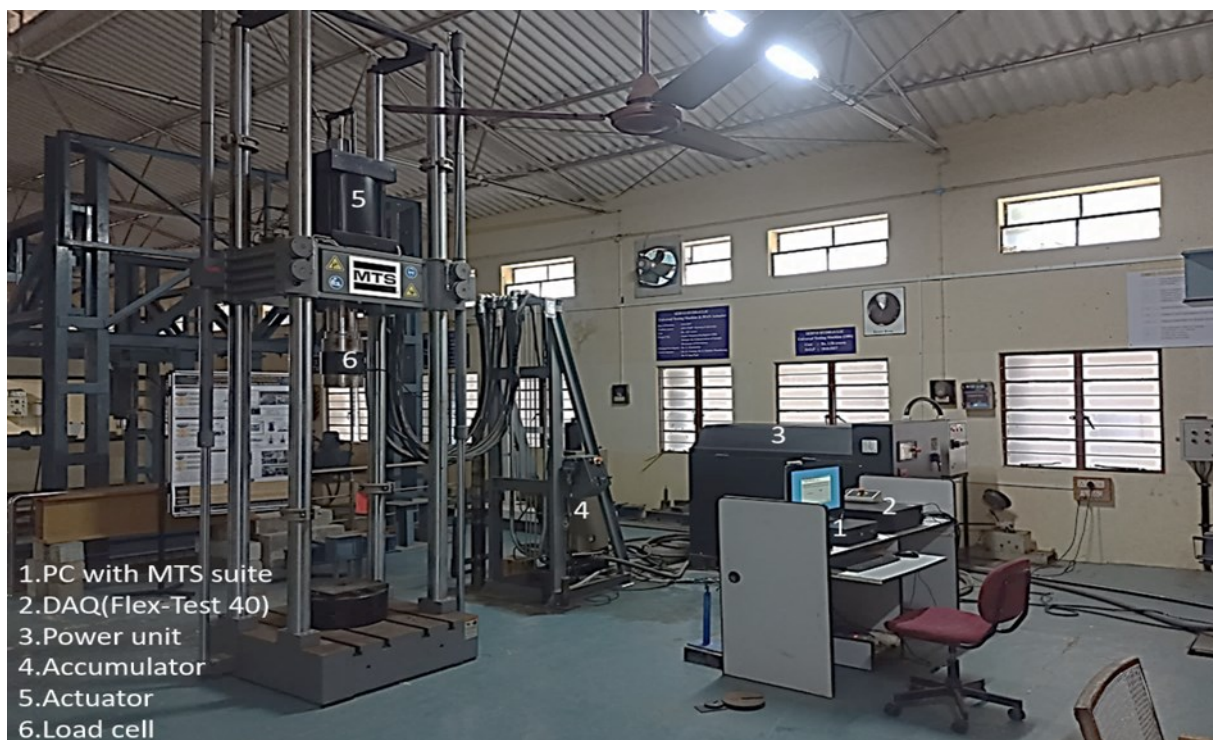
Figure 6. Experimental set up using a 311,31 MTS servo-hydraulic UTM

The prototype MRD was fabricated according to the dimensions in Table 1 and the FEM model. Figure 7(a) shows the MRD's components. MRF flows through the piston-cylinder clearance in the damper from the upper to lower chambers. In the Structural Engineering Laboratory, the prototype MRD was filled with LORD-MRF132DG in both chambers and then tested using the Servo-hydraulic MTS-UTM.

The MRD was tested on the MTS servo-hydraulic system, which was mounted in the centre of the load cell and the cast-iron base, as shown in Figure 7(b). After testing, the MTS Test Suite software generated force-time, time-displacement, and force-displacement graphs. The built-in software MTS Test Suite was used to control the test. Real-time data on force, displacement, and time were collected and analysed for different frequencies using the experimental setup with the MRD. The MRD's performance was categorized based on displacement and frequency.
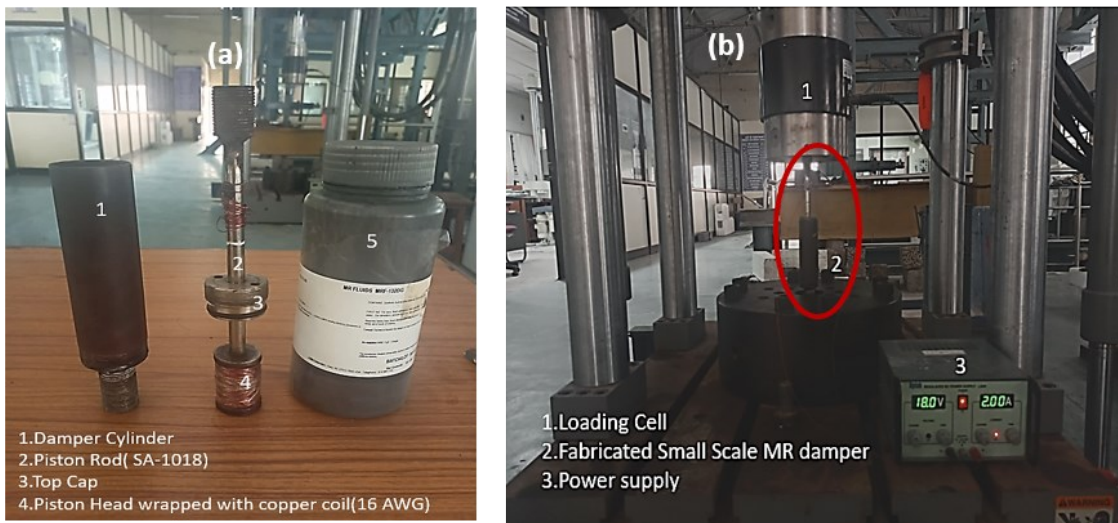
Figure 7. a) Components of designed and fabricated small-scale MRD;

b) damper installation in MTS

The test was carried out for 10 cycles with a maximum displacement of 15 mm in the MRD and an excitation frequency of 1 Hz. Following the Multiphysics simulation, the piston was wrapped with 500 turns of copper coil (16-AWG) and supplied with a varying DC input value of 0,5 to 2,0 A in increments of 0,5 A. The DC supply was set to 0,5; 1,0; 1,5, and 2,0 A using the test suit software, with a 15 mm stroke length cyclic excitation. The force versus displacement curve was used to analyse the dynamic behaviour of the MRD.
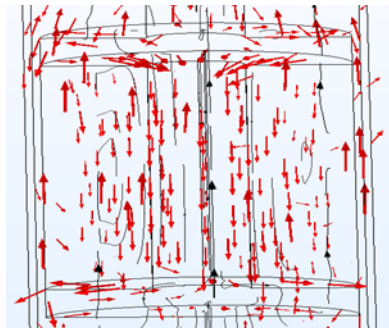

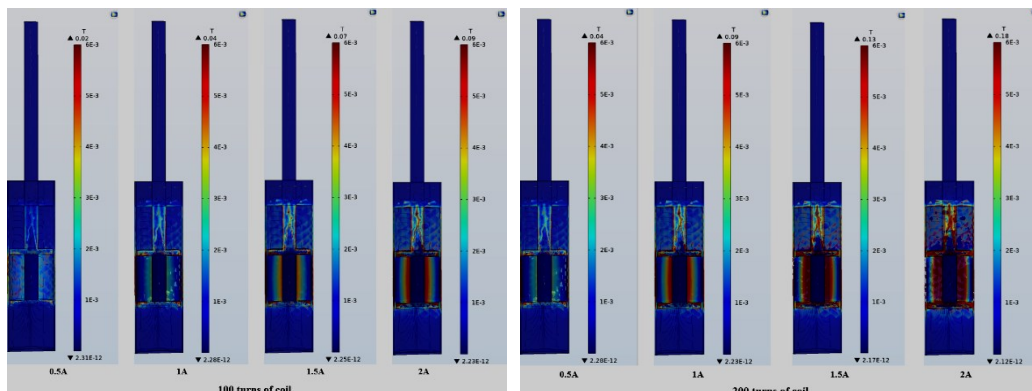**Figure 8. MF lines in the piston of the MRD model**

Figure 9. Magnetic flux density induced by varying current for 100 and 200 coils
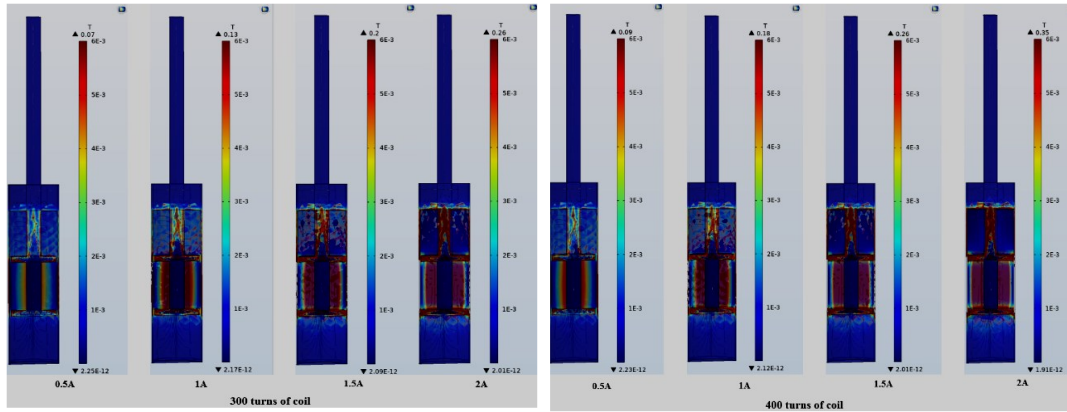
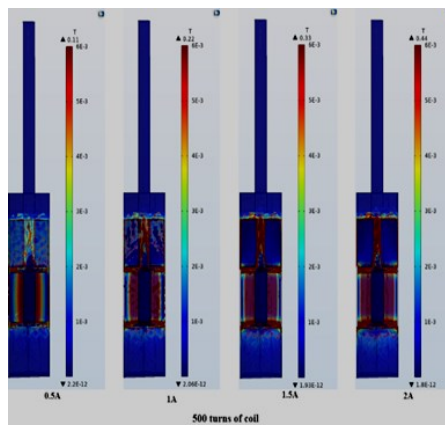**Figure 10. Magnetic flux density induced by varying current for 300 and 400 coils**

Figure 11. Magnetic flux density induced by varying current for 500 coils

Table 2. Damping force corresponding to MF density and number of coils

Coil turns	Induced current (A)	Magnetic flux (T)	Force (N)
100	0,5	0,02	307,90
	1,0	0,05	439,40
	1,5	0,07	513,60
	2,0	0,09	578,80
200	0,5	0,05	439,40
	1,0	0,09	578,80
	1,5	0,13	708,29
	2,0	0,18	798,41
300	0,5	0,07	513,60
	1,0	0,13	708,29
	1,5	0,20	825,53
	2,0	0,26	890,52
400	0,5	0,09	578,81
	1,0	0,18	798,41
	1,5	0,26	890,52
	2,0	0,35	939,43
500	0,5	0,11	671,77
	1,0	0,22	805,69
	1,5	0,33	922,54
	2,0	0,44	989,36

Table 3. Damping force with a similar magnetic flux density and variation in coil numbers

| Magnetic flux (T)	Damping Force (N)	Similarity
0,05	439,40	100 coils with 1A and 200 coils with 0,5A
0,07	513,60	100 coils with 1,5A and 300 coils with 0,5A
0,09	578,80	100 coils with 2A, 200 coils with 1A and 400 coils with 0,5A
0,13	708,29	200 coils with 1,5A and 300 coils with 1A
0,18	798,29	200 coils with 2A and 400 coils with 1A
0,26	890,52	300 coils with 2A and 400 coils with 1,5A

The relationship between the number of coils and the input current used in the piston and the generation of DF is presented in Table 2. It has been found that a smaller number of coils with a higher current can produce the same MF and DF as a larger number of coils with a lower current. For example, 100 coils with a current of 1 A produce 0,05 T, resulting in a DF of 439,4 N. This is equivalent to the DF produced by 200 coils with a 0,5 A current. Such examples can be seen in Table 3, which contains the simulation results. Similar results on how the current affects the MF in the damper can be observed in the studies conducted by Purandare et al. [22], T. M. Gurubasavaraju et al. [27], and Guoliang Hu et al. [31]. It has also been found that as the number of turns on the coil and the current increase, so do the MF and DF (Figures 12 and 13). Maximum MF was achieved at 2 A current and various coil turns. Based on the data collected, it is possible to conclude that the relationship between the MF generated by the number of coil turns and the current, MF, and DF generated is directly proportional. By applying a current of 2 A to 500 turns of the coil, the simulation produced a maximum DF of 989,36 N, resulting in an MF of 0,44 T. The overall increase in MF and DF is presented in Table 4.
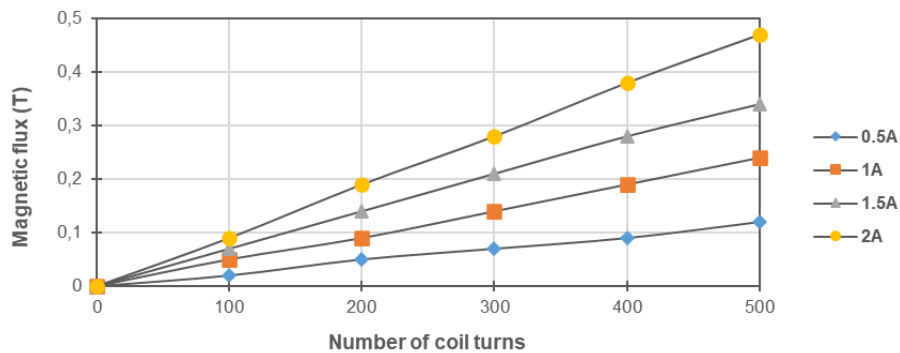

Figure 12. MF generated by current input and coil
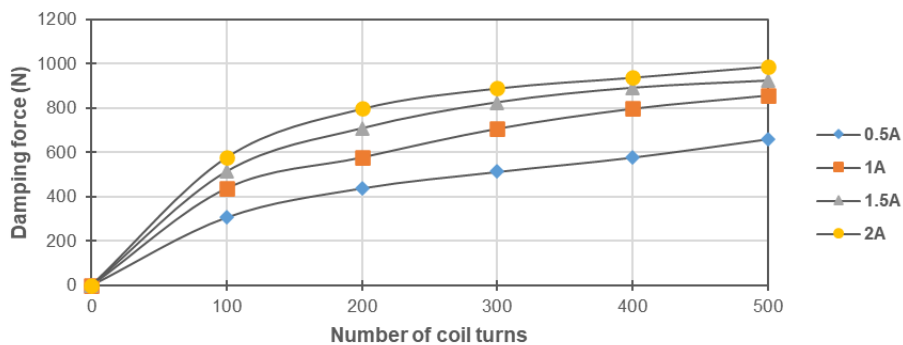
Figure 13. Damping force generated by current input and coil

Table 4. Increase in DF and MF

| Current induced (A)	Coil numbers	% of magnetic flux increased	% of damping force increased
0,5	200	60,00	29,92
	300	71,43	40,05
	400	77,78	46,80
	500	83,34	53,47
1,0	200	44,45	24,08
	300	64,29	37,96
	400	73,70	44,96
	500	79,17	48,81
1,5	200	50,00	27,48
	300	66,67	37,78
	400	75,00	42,32
	500	79,41	44,32
2,0	200	52,63	27,50
	300	67,86	35,00
	400	76,31	38,39
	500	80,85	41,49

Based on the numerical model, 500 turns of the copper coil and varying currents from 0,5 to 2,0 A were used for the validation. The experiment was performed with 15 mm displacement and a fixed frequency of 1 Hz. The built-in DAQ system (Flextest-40) of the MTS suite recorded the experimental DF, piston rod displacement, and time for completion for the specified number of cycles. The MRF had to be filled with care to avoid air bubbles. The annular gap controlled the flow of fluid between the chambers. Depending on the first starting stroke, MRF flowed from the upper chamber to the lower chamber as the piston rod of the MRD began to excite. It was assumed that the compression stroke would be the negative cycle and the positive stroke would be the positive cycle. Upon excitation, the volume displaced by the piston rod equalled the fluid flow over the annular gap from the upper reservoir to the lower reservoir. The force-displacement relationship for the entire cycle is presented in Figure 14 for a range of currents while keeping the displacement at 15 mm and a constant frequency excitation at 1 Hz. It was observed that the force produced by 15 mm piston displacement increased with its velocity. When the frequency was high, the size of the F-D plot in the area right before yielding increased noticeably. The smooth curve of the F-D plot shown in Figure 15 was due to the absence of air bubbles inside the MRD, possibly due to the careful filling of MRF in the chamber. Similar smooth curves were observed [44-47].
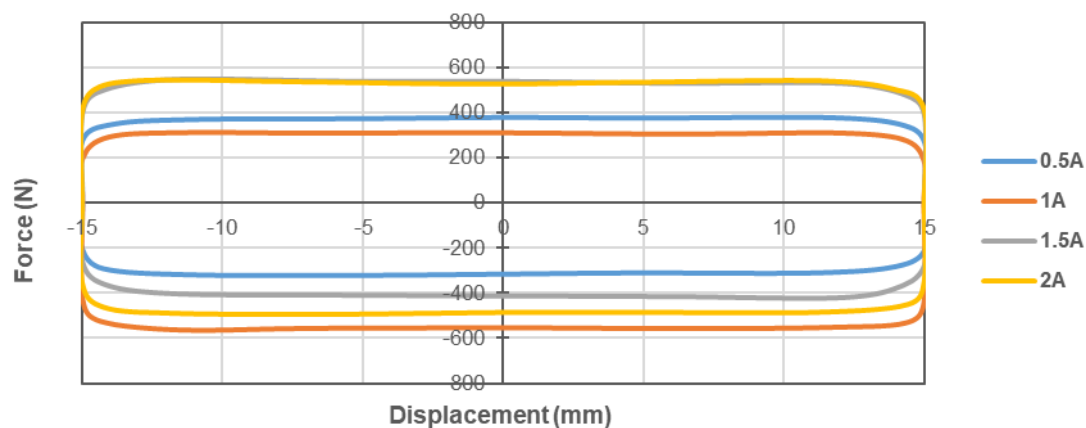
**Figure 14. Force-displacement plot for a displacement of 15 mm**
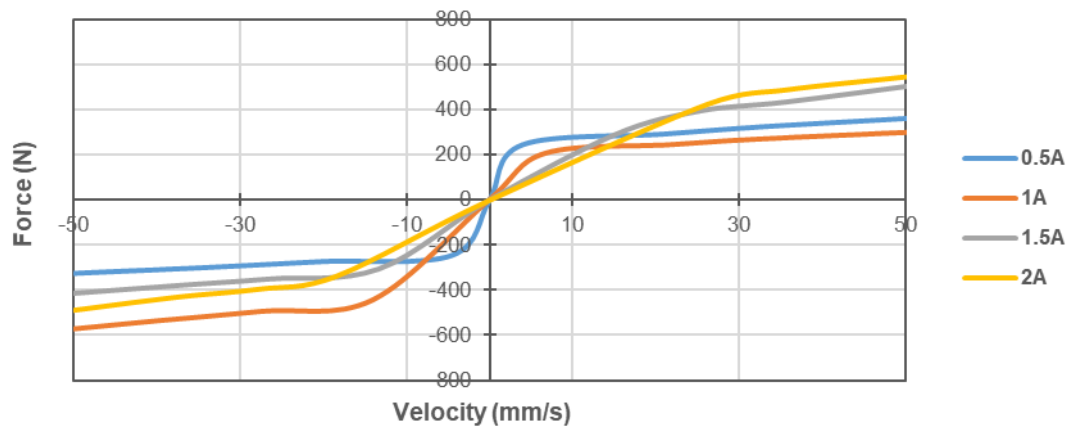
Figure 15. Force-velocity plot for a displacement of 15 mm

The test was executed as displacement and excitation frequency control with current fluctuation. Hence, the relationship between frequency excitation and velocity was established manually from real-time data collected by the DAQ system. Figure 15 shows a velocity plot of the data collected for all negative and positive cycles. The velocity of the piston was estimated using real-time data from a DAQ system connected to a computer via MTS Suite and was found to be 52,284 mm/s for the excitation frequency of 1 Hz. The velocity profile was assumed to remain unchanged during the experiment even though the current was varied. It was also observed that the positive and negative cycle forces increased as the current increased while keeping the same velocity of 52,284 mm/s.
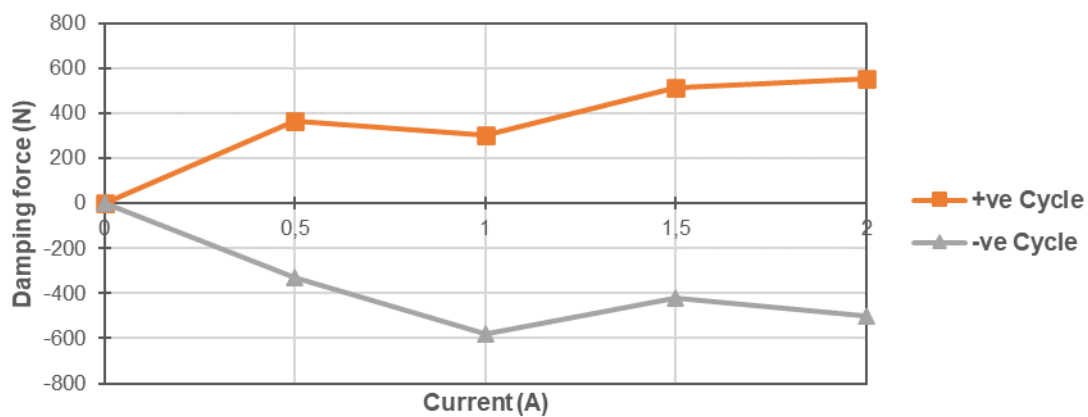

Figure 16. DF for varying current

The response forces resulted in two distinct cycles due to the excitation frequency, namely a negative cycle when the piston moved downwards and a positive cycle when the piston moved upwards. Maximum forces for the negative cycle were recorded as 330,69; 582,27; 419,35; and 448,29 N for currents of 0,5; 1,0; 1,5 and 2,0 A, respectively. Similarly, for the positive cycle, maximum forces were 368,56; 301,43; 512,28 and 556,34 N for currents of 0,5; 1,0; 1,5 and 2,0 A, respectively. The variation in damping forces in different cycles is plotted in Figure 16 for clarity. Variations in forces occurred in response to increases in current caused by shear thinning and shear thickening inside the MRD. A similar phenomenon has been reported [45-50]. It was also inferred from Figure 13 that maximum damping force was developed in the negative cycle, i.e., when the piston was moving downwards, which corresponded to the shear thickening phenomenon governing this study.
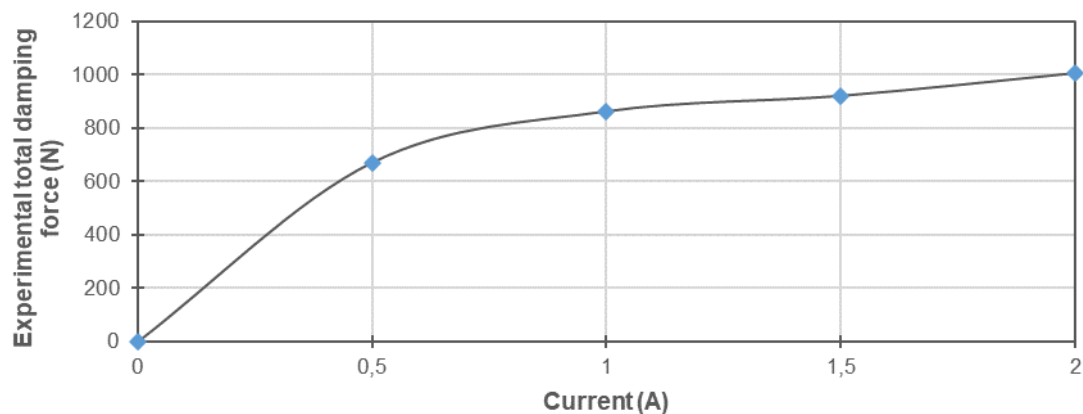
Figure 17. Total DF for varying current

The total DF produced by the small-scale MRD was the sum of the maximum forces acting in the negative and positive cycles throughout the test [48-52]. Figure 17 shows the overall DF produced by the small-scale MRD with a maximum displacement of 15 mm under various current conditions. Maximum DF of 699,25; 833,43; 931,63; 1004,63 N were observed for currents of 0,5; 1,0; 1,5 and 2,0 A, respectively. It was also inferred from the plot that fixed excitation frequency and displacement resulted in increased DFs with increased current. As the current increased, the DF of the designed small-scale MRD increased noticeably.
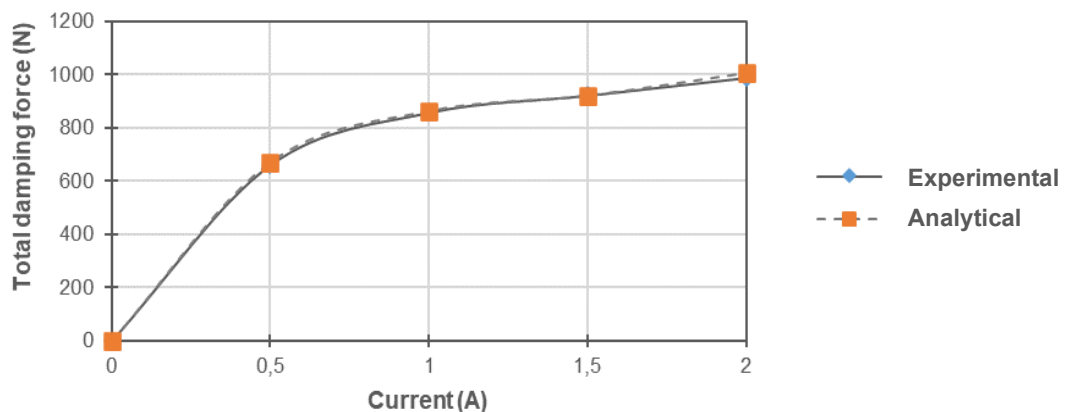

Figure 18. Comparison between the experimental and analytical models

The overall DF of the developed MRD was compared to the analytical results obtained using the numerical solution and FEM solution. Figure 18 compares experimental and analytical model data to confirm comparable behaviour that showed the force increased with increased current. Similar to [45] the analytical and experimental model curves were smooth and grew similarly, although an error percentage of less than 5 was observed. The percentage of error in total DF for the analytical and experimental model is presented in Table 6. To summarize, one of the most notable findings of this study was that increasing the coil turn and current for constant frequency excitation resulted in an increase in the associated DF, which was related to a higher velocity and damping coefficient. The FEM (COMSOL) model produced 989,36 N at 1 Hz, while the experimental model produced 1004,63 N.

According to [52, 53] one simple approach to reducing structural vibration is the installation of extra-damping devices. This technique uses the structure's natural motion to generate displacements within the MRD's part. These devices should respond by applying strong DFs, distributing energy evenly across the system [49]. Experiments were conducted in which a

constant sinusoidal excitation, constant displacements, and varying current were used to investigate the energy dissipation caused by the newly constructed small-scale MRD.
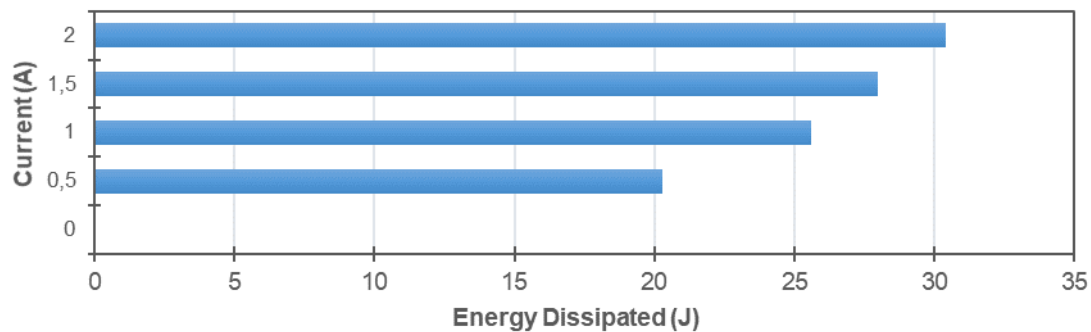
Figure 19. Energy dissipation in MRD

The total energy absorbed by the MRD devices during a typical vibration cycle while the MRD was operating in a constant magnetic field was used to evaluate the effectiveness of the small-scale MRD. This calculation was done with the MRD operating in a constant magnetic field [54]. The MRD formed a hysteresis closed-loop force-displacement curve, allowing efficient cyclic energy dissipation across all varying currents [51-54]. The energy dissipation of the designed small-scale MRD was computed as a single cycle using the area enclosed by a hysteresis closed loop [44, 46] and an average of 10 complete cycles at 1 Hz, 15 mm, and 0,5-2,0 A. A hysteresis F-D closed loop was used for calculating energy dissipation. Figure 19 shows the energy dissipated at the highest cycle among the 10 cycles with varied currents generated for 15 mm displacement. Figure 19 shows that energy dissipation increased with current. The small-scale MRD could control structure vibrations with this information.

For the maximum displacement of 15 mm available in the MRD and excitation frequency of 1 Hz, the energy dissipation ranged from 20,89; 25,62; 27,98 and 30,38 J, corresponding to currents of 0,5; 1,0; 1,5 and 2,0 A, respectively. Energy dissipation was proportional to current, with a maximum increase observed when the current was increased while displacement and excitation frequency remained constant at 15 mm and 1 Hz.

The validated results for the small-scale MRD in the present study were compiled for clarity in Table 5.

Table 5. Compiled results for the developed MRD

Coil turns	Current	DF Numerical (N)	DF (+Ve)	DF (-Ve)	DF Experimental (N)	% Variation	Energy dissipated (J)
500	0,5	671,77	330,69	368,56	699,25	3,92	20,89
	1,0	805,69	582,27	301,43	833,43	3,33	25,62
	1,5	922,54	419,35	512,28	931,63	1,01	27,98
	2,0	989,36	448,29	556,34	1004,63	1,51	30,38

4 Experimental testing of reinforced concrete frames with and without MRDs

The test specimen in this investigation was a reduced-scale (1:3) single-story and single-bay RC frame similar to an internal bay at the ground-story level of the prototype frame. The support condition of the specimen was fixed, and seismic load was applied. All members of the prototype frame were designed and detailed according to the Indian Standards provisions IS 456:2021. High-yield strength Fe-500 steel bars were used for the longitudinal and transverse reinforcement of all specimens. The yield strength and ultimate strength of longitudinal and transverse steel bars were 554,65 N/mm^2 and 670,69 N/mm^2, respectively,

for 8 mm diameter rods and 557,26 N/mm^2 and 676,84 N/mm^2, for 10 mm diameter rods, as per the specifications in the IS456:2021 code. The frame was constructed using an M20 mix design in accordance with the specifications in IS 10262:2019. The properties of materials used in casting frames are presented in Tables 6-9. The dimensions and detailing of the reinforced concrete (RC) frame are shown in Figure 20.

Table 6. Properties of PPC

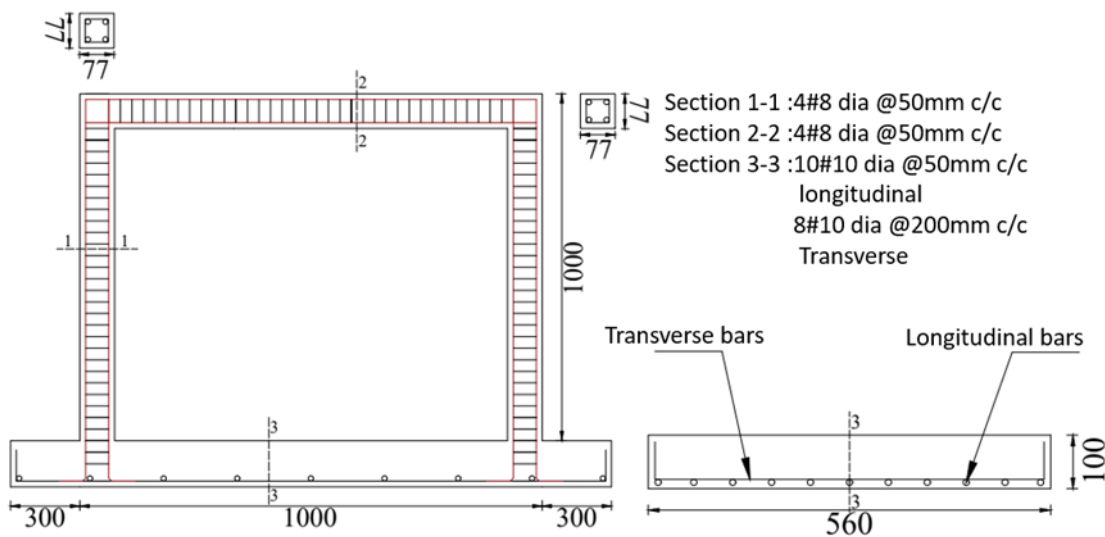| Physical properties	Observed values	Desired values
Standard consistency	28,5 %	—
Initial setting time	130 min	> 30 min
Final setting time	225 min	< 600 min
Compressive strength 3 day	28,1 MPa	> 23 MPa
7 day	38,3 MPa	> 33 MPa
28 day	48,1 MPa	> 43 MPa

Table 7. Physical properties of the aggregates

Property	Coarse aggregate	Fine aggregate
Specific gravity	2,700	2,65
Water absorption (%)	0,340	1,12
Bulk density (kg=m^3)	1,485	1,62

Table 8. Properties of rebar

Size	Yield Strength (N/mm^2)	Ultimate Strength (N/mm^2)	Elongation (%)
8mm	554,65	670,69	20,53
10mm	557,26	676,84	25,81

Table 9. Mix design for M20

Materials	Quantity
Cement	396,62
Fine Aggregates	572,69
Coarse Aggregates	1172,86
Water	189,91

Section 1-1 :4#8 dia @50mm c/c
Section 2-2 :4#8 dia @50mm c/c
Section 3-3 :10#10 dia @50mm c/c
        longitudinal
   8#10 dia @200mm c/c
        Transverse

Figure 20. Geometric properties of the RC frames [dimensions in mm]

Figure 21. RC frames tests: a) without damper; b) with MRD

Two tests based on cyclic loading were conducted to investigate the effect of inserting an MRD in the frame. Figure 21 shows the experimental setup for an RC frame with and without a single MRD at L/3 from the beam-column. The setup included a lateral load applied to the beam level RC frame and cyclic forces mainly affecting the floor level through the hydraulic actuator. The actuator had a compressive or tensioning force of 50 kN and a stroke of 125 mm. The loading frame had a capacity of 250 kN. Transducers in the MTS (FLEXTEST-40) DAQ system measured actuator piston force and displacement.

For cyclic loading, an actuator and LVDTs were used. The actuator measured the lateral force applied to the frame, while LVDTs at the column midpoints measured the displacement response. The actuator moved in 25 mm increments, and the LVDT tip was 50 mm from the column face. LVDTs were located along the height of the frame columns for all specimens, as shown in Figure 21.
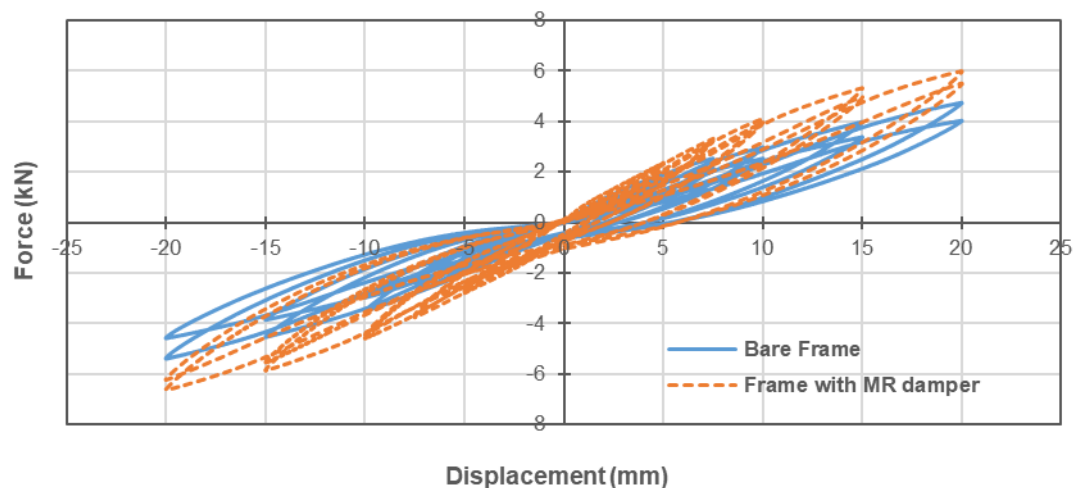
Figure 22. Force-displacement response of the tested frames

The tests showed that placing an MRD on the frame increased its load-carrying capacity. The cyclic test found that a frame with an MRD performed better than a bare frame by showing higher load-carrying capacity. Figure 22 shows the force-displacement curve based on the experimental observations for frames with and without an MRD. This vibration control method increased the ultimate load-carrying capacity of a frame with MRD compared to a bare frame specimen. The maximum load-carrying capacity of the frame with an MRD was 5,99 kN during positive cycles and 6,62 kN during negative cycles. This was 20,16 % higher for the positive cycle and 18,82 % higher for the negative cycle than the load-carrying capacity of a bare frame. The ultimate load-carrying capacity for the bare frame and the frame with the MR damper was

10,03 kN and 12,61 kN, respectively, representing a 19,49 % overall increase in load-carrying capacity.

The stiffness degradation of the specimens was analysed, and it was found that the initial stiffness of the frame with MRD was higher than that of the bare frame specimen. The experimental test showed a maximum stiffness of 0,479 for the frame with MRD and 0,346 for the bare frame. The highest stiffness was observed when the displacement reached 5 mm (initial), but it decreased as both the displacement and the number of cyclic excitations increased. Figure 23 shows the plot of the stiffness degradation in the specimens. The energy dissipating (ED) capability of a structure is important for evaluating its performance under seismic excitations. Therefore, ED without significant loss of stiffness or strength indicates the structure's capability. A structure can dissipate more energy by providing enough inelastic deformation in a critical area, enough connection ductility, or adding additional devices. The ED capacity is defined as the area under the hysteresis loop for each load cycle. Cumulative ED can be calculated from the maximum area under the force-displacement curves of test specimens [55, 56]. Figure 24 shows the cumulative energy dissipated by both frames.

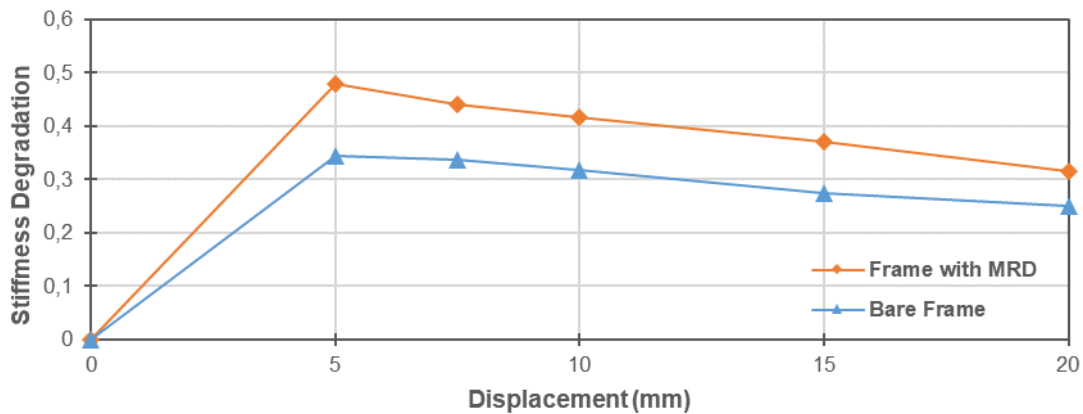**Figure 23. Stiffness degradation of the tested frames**
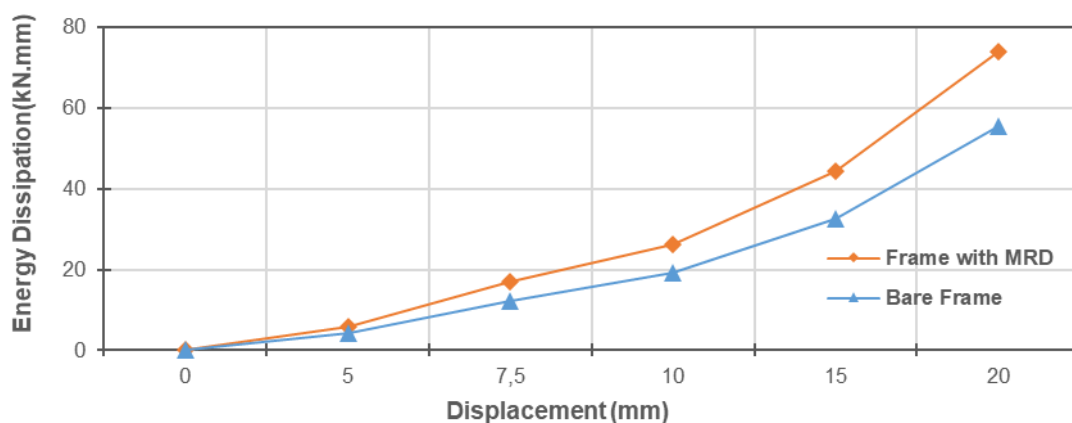

Figure 24. Energy dissipation in the tested frames

Table 10 presents the load-carrying capacity and energy dissipation results of the two tested frames with a comparison of results.

Table 10. Compiled results for tested frames

Specimen	+ve Cycle (kN)	-ve Cycle (kN)	ED (kNmm)	Cumulative Increased Force (%)	Cumulative Increased ED (%)
Bare Frame	4,74	-5,29	55,52	0,00	0,00
Frame with MR damper	5,99	-6,62	73,95	19,49	24,92

5   Conclusions

This study demonstrates the potential of using COMSOL software to model and optimize MRD for vibration control in structural applications. The findings show that optimizing various parameters, such as coil turns and current, can achieve the maximum MF value in the MRD. MRDs are known for their ability to provide adaptive and controllable damping characteristics, making them highly suitable for applications that require precise control over vibrations and displacements.

- o   The analytical simulation shows that the MF density is directly proportional to the number of coil turns and induced current. A maximum MF of 0,44 T was generated with 500 turns of coils and 2,0 A induced current.
- o   The maximum damping force at 2,0 A with 500 turns of coils was 1004,63 N for the experimental model and 989,36 N for the analytical model, with a difference of 1,54 %.
- o   The highest energy dissipated by the MRD with 2,0 A and 500 turns of coils was 30,38 J, which is 31,23 % higher than that of the MRD with 0,5 A and 500 coils.
- o   With an MRD, the frame could carry 5,99 kN during positive cycles and 6,62 kN during negative cycles.
- o   An MRD increases the positive cycle load-carrying capacity by 20,16 % and the negative cycle by 18,82 %.
- o   The frame with the MRD has a 19,49 % cumulative increase in load-carrying capacity from 4,74 to 5,99 kN in the negative cycle and from 5,29 to 6,62 kN in the positive cycle.
- o   The frame with the MRD has a 24,92 % cumulative increase in energy dissipation, from 53,52 to 75,95 kNmm.

The study's experimental and numerical results agree with the developed MRD, indicating the model's accuracy. When incorporated in the Reinforced cement concrete frame (RCC), the frame with MRD performs significantly better than the bare frame, which directly implies the advantages of MRD in the frame structure. This research provides valuable insights into the optimization and validation of MRD, which can lead to their better performance in practical applications in civil engineering structures.

Future research on the current investigation could entail the utilization of a greater number of MRD positioned at various locations within the framework rather than confining them solely to the current placement site. Implementing and using different accumulator mechanisms can significantly enhance the performance of the MRD and frame specimens.

Abbreviations

A	Ampere
DF	Damping Force
FD	Force displacement
FEM	Finite Element Method
MC	Magnetic Circuit
MF	Magnetic Flux density
MRD	Magnetorheological Damper
MRF	Magnetorheological Fluid
T	Tesla

Acknowledgments

References

[1]   Chopra, A. K. Dynamics of structures Theory and Applications to Earthquake Engineering. 4th edition, New Jersey, USA: Pearson Education, 2013.

[2]   Symans, M. D.; Constantinou, M. C. Semi-active control systems for seismic protection of structures: A state-of-the-art review. Engineering Structures, 1999, 21 (6), pp. 469-487. https://doi.org/10.1016/S0141-0296(97)00225-3

[3]   Symans, M. D.; Constantinou, M. C. Seismic testing of a building structure with a semi-active fluid damper control system. Earthquake Engineering and Structural Dynamics, 1998, 26 (7), pp 759-777. https://doi.org/10.1002/(SICI)1096-9845(199707)26:7<759::AID-EQE675>3.0.CO;2-E

[4]   Spencer Jr., B. F.; Dyke, S. J.; Sain, M. K.; Carlson, J. D. Phenomenological model for magnetorheological dampers. Journal of Engineering Mechanics, 1997, 123 (3), pp. 230-238. https://doi.org/10.1061/(ASCE)0733-9399(1997)123:3(230)

[5]   Venanzi, I. A review on adaptive methods for structural control. Open Civil Engineering Journal, 2016, 10, pp. 653-667. https://doi.org/10.2174/1874149501610010653

[6]   Basili, M.; De Angelis, M. Vibration analysis and models of adjacent structures controlled by magnetorheological dampers. Shock and Vibration, 2017, 2017. https://doi.org/10.1155/2017/9596382

[7]   Dyke, S. J.; Spencer Jr., B. F.; Sain, M. K.; Carlson, J. D. Experimental verification of semi-active structural control strategies using acceleration feedback. In: Proceedings of the 3rd International Conference on Motion and Vibration Control. 1-6 September 1996, Chiba, Japan, pp. 291-296.

[8]   Christenson, R.; Lin, Y. Z.; Emmons, A.; Bass, B. Large-scale experimental verification of semiactive control through real-time hybrid simulation. Journal of Structural Engineering, 2008, 134 (4), pp. 522-534. https://doi.org/10.1061/(ASCE)0733-9445(2008)134:4(522)

[9]   Javanmardi, A. et al. Application of structural control systems for the cables of cable-stayed bridges: State-of-the-art and state-of-the-practice. Archives of Computational Methods in Engineering, 2022, 29, pp. 1611-1641. https://doi.org/10.1007/s11831-021-09632-4

[10]   Yang, G.; Spencer Jr., B. F.; Carlson, J. D.; Sain, M. K. Large-scale MR fluid dampers: modeling and dynamic performance considerations. Engineering Structures, 2002, 24 (3), pp. 309-323. https://doi.org/10.1016/S0141-0296(01)00097-9

[11]   Dyke, S. J.; Spencer Jr., B. F.; Sain, M. K.; Carlson, J. D. An experimental study of MR dampers for seismic protection. Smart Materials and Structures, 1998, 7 (5), pp. 693-703. https://doi.org/10.1088/0964-1726/7/5/012

[12]   Chaudhuri, P.; Maity, D.; Maiti, D. K. Investigation of a diagonal magnetorheological damper for vibration reduction. Journal of Vibration Engineering and Technologies, 2022, 10, pp. 1451-1471. https://doi.org/10.1007/s42417-022-00458-3

[13]   Jung, H.-J. et al. MR damper-based smart passive control system for seismic protection of building structures. In: Proceedings Volume 6174, Smart Structures and Materials 2006: Sensors and Smart Structures Technologies for Civil, Mechanical, and Aerospace Systems, Tomizuka, M.; Yun, C.-B.; Giurgiutiu, V. (eds.). 26 February 2 March 2006, San Diego, California, USA, SPIE Digital Library. https://doi.org/10.1117/12.657927

[14]   Prado, M. R. G. Modeling and simulation of magnetorheological dampers for the reduction of the seismic response of structures using simulink. Tecnia, 2022, 32 (2), pp. 36-46. https://doi.org/10.21754/tecnia.v32i2.1402

[15] Rabinow, J. The magnetic fluid clutch. Transactions of the American Institute of Electrical Engineers, 1948, 67 (2), pp.1308-1315. https://doi.org/10.1109/T-AIEE.1948.5059821

[16] Wang, D. H.; Liao, W. H. Semiactive controllers for magnetorheological fluid dampers. Journal of Intelligent Material Systems and Structures, 2005, 16 (11-12), pp. 983-993. https://doi.org/10.1177/1045389X05055281

[17] Zhang, R.-H.; Soong, T. T. Seismic design of viscoelastic dampers for structural applications. Journal of Structural Engineering, 1992, 118 (5), pp. 1375-1392. https://doi.org/10.1061/(ASCE)0733-9445(1992)118:5(1375)

[18] Rashid, M. M.; Hussain, M. A.; Rahim, N. A. Application of Magnetorheological damper for Car Suspension Control. Journal of Applied Sciences, 2006, 6 (4), pp. 933-938. https://doi.org/10.3923/jas.2006.933.938

[19] Kumar, A.; Mangal, S. K. Properties and applications of controllable fluids: A review. International Journal of Mechanical Engineering Research, 2012, 2 (1), pp. 57-66.

[20] Biswal, T.; Rao, L. B. Analysis of the magnetic field for MRD working in shear mode. International Journal of Structural Engineering, 2015, 7 (1), pp. 48-62. https://doi.org/10.1504/IJSTRUCTE.2016.073678

[21] Gurubasavaraju, T. M.; Hemantha, K.; Arun, M. A study of influence of material properties on MF density induced in magneto rheological damper through FE analysis. In: International Conference on Research in Mechanical Engineering Sciences (RiMES 2017) MATEC Web of Conferences, 144, 2018. https://doi.org/10.1051/matecconf/201814402004

[22] Purandare, S.; Zambare, H.; Razban, A. Analysis of Magnetic Flux in magneto-rheological damper. Journal of Physics Communications, 2019, 3 (7). https://doi.org/10.1088/2399-6528/ab33d7

[23] Li, G.; Yang, Z.-B. Modelling and analysis of a magnetorheological damper with non-magnetized passages in piston and minor losses. Shock and Vibration, 2020, pp. 1–12. https://doi.org/10.1155/2020/2052140

[24] Liu, L. et al. Performance Analysis of Magnetorheological Damper with Folded Resistance Gaps and Bending Magnetic circuit. Actuators, 2022, 11 (6). https://doi.org/10.3390/act11060165

[25] Elsaady, W.; Olutunde Oyadiji, S.; Nasser, A. A one-way coupled numerical magnetic field and CFD simulation of viscoplastic compressible fluids in MRDs. International Journal of Mechanical Sciences, 2020, 167. https://doi.org/10.1016/j.ijmecsci.2019.105265

[26] Ganesha, A.; Patil, S.; Kumar, P. N.; Murthy, A. Magnetic field enhancement technique in the fluid flow gap of a single coil twin tube Magnetorheological damper using magnetic shields. Journal of Mechanical Engineering and Sciences JMES, 2020, 14 (2), pp. 6679-6689.

[27] Gurubasavaraju, T. M.; Kumar, H.; Mahalingam, A. An approach for characterizing twin-tube shear-mode magnetorheological damper through coupled FE and CFD analysis. Journal of the Brazilian Society of Mechanical Sciences and Engineering, 2018, 40. https://doi.org/10.1007/s40430-018-1066-z

[28] Cheng, M.; Chen, Z. B.; Xing, J. W. Design, analysis, and experimental evaluation of a magnetorheological damper with meandering magnetic circuit. IEEE Transactions on Magnetics, 2018, 54 (5). https://doi.org/10.1109/TMAG.2018.2797090

[29] Aziz, M. A.; Aminossadati, S. M.; Leonardi, C. Load response of magnetorheological (MR) plastomer dampers under applied magnetic fields. Journal of Magnetism and Magnetic Materials, 2022, 547. https://doi.org/10.1016/j.jmmm.2021.168930

[30] Shiao, Y.; Kantipudi, M. B. Multi-physics analysis of a magnetorheological valve train with experimental validation. Applied Sciences, 2022, 12 (18). https://doi.org/10.3390/app12189109

[31]   Hu, G. et al. Geometric optimization and performance analysis of radial MR valve using Taguchi orthogonal experiment method. Journal of Mechanical Science and Technology, 2022, 36, pp. 4593-4614. https://doi.org/10.1007/s12206-022-0822-2

[32]   Yang, Y. et al. Performance tests and microstructure-based sigmoid model for a three-coil magnetorheological damper. Structural Control and Health Monitoring, 2021, 28 (11). https://doi.org/10.1002/stc.2819

[33]   Gurubasavaraju, T. M. Estimation of DF of double Ended Magnetorheological Damper through one way coupled CFD and FEA Analysis. Journal of the Institution of Engineers (India): Series C, 2021, 102, pp. 1145-1151. https://doi.org/10.1007/s40032-021-00737-0

[34]   Vivekananda Sharma, S.; Hemalatha, G.; Ramadevi, K. Analysis of magnetic field-strength of multiple coiled MR-damper using comsol multiphysics. Materials Today: Proceedings, 2022, 66 (4), pp. 1789-1795. https://doi.org/10.1016/j.matpr.2022.05.279

[35]   Singla, R. Design of a mixed-mode MRD with reduced off-state damping. [honors theses], Ohio State University, Department of Mechanical Engineering, Ohio, USA, 2005. Accessed: 4 October 2023. Available at: https://kb.osu.edu/handle/1811/5849

[36]   Jolly, M. R.; Bender, J. W.; Carlson, J. D. Properties and applications of commercial magnetorheological fluids. In: Proceedings Volume 3327, Smart Structures and Materials 1998: Passive Damping and Isolation, Davis, L P. (ed.). 1-5 March 1998, SPIE Digital Library. https://doi.org/10.1117/12.310690

[37]   COMSOL. AC/DC module Simulate Low-Frequency Electromagnetics and Electromechanical Components. Accessed: 15 May 2023. Available at: https://www.comsol.com/acdc-module

[38]   Abdul Aziz, M.; Mohtasim, S. M.; Ahammed, R. State-of-the-art recent developments of large magnetorheological (MR) dampers: a review. Korea-Australia Rheology Journal, 2022, 34, pp. 105-136. https://doi.org/10.1007/s13367-022-00021-2

[39]   Lenggana, B.W. et al. Review of Magnetorheological Damping Systems on a Seismic Building. Applied Sciences, 2021, 11 (19). https://doi.org/10.3390/app11199339

[40]   Xu, Z.-D.; Jia, D.-H.; Zhang, X.-C. Performance tests and numerical model considering magnetic saturation for magnetorheological damper. Journal of Intelligent Material Systems and Structures, 2012, 23 (2), pp. 1331-1349. https://doi.org/10.1177/1045389X12445629

[41]   Parker. Lord Division. Accessed: 11 February 2023. Available at: http://www.lord.com/

[42]   Wang, X; Gordaninejad, F. Dynamic modelling of semi-active ER/MRF dampers. In: Proceedings Volume 4331, Smart Structures and Materials 2001: Damping and Isolation, Inman D. J. (ed.). 4-8 March 2011, SPIE Digital Library; pp. 82–91. https://doi.org/10.1117/12.432736

[43]   Jiang, X.; Wang, J.; Hu, H. Designing and modeling of a novel magneto-rheological fluid damper under impact load. In: Proceedings of the 3rd ICMEM International conference on Mechanical Engineering and Mechanics. 19-25 October 2009, Beijing, China, 2009, pp. 203-207.

[44]   Dixon, J. C. The shock absorber handbook. 2nd edition, John Willey & Sons Ltd., 2007.

[45]   Vivekananda Sharma, S.; Hemalatha, G. Numerical and experimental investigation on small scale magnetorheological damper. International Journal of Engineering, 2022, 35 (12), pp. 2395-2402. https://doi.org/10.5829/IJE.2022.35.12C.16

[46]   Rendos, A. et al. Shear thickening prevents slip in magnetorheological fluids. Smart Materials and Structures, 2020, 29 (7). https://doi.org/10.1088/1361-665X/ab8b2e

[47]   Sapiński, B.; Horak, W. Rheological properties of MR fluids recommended for use in shock absorbers. Acta Mechanica et Automatica, 2013, 7 (2)m pp. 107-110. https://doi.org/10.2478/ama-2013-0019

[48]   Weber, F.; Distl, H.; Feltrin, G.; Motavalli, M. Cycle energy control of magnetorheological dampers on cables. Smart Materials and Structures, 2009, 18 (1). https://doi.org/10.1088/0964-1726/18/1/015005

[49]   Jacob, K.; Tan, A. S.; Sattel, T.; Kohl, M. Enhancement of shock absorption using hybrid SMA-MRF damper by complementary operation. Actuators, 2022, 11 (10). https://doi.org/10.3390/act11100280

[50]   Dimock, G. A.; Lindler, J. E.; Wereley, N. M. Bingham biplastic analysis of shear thinning and thickening in magnetorheological dampers. In: Proceedings Volume 3985, Smart Structures and Materials 2000: Smart Structures and Integrated Systems, Wereley, N. M. (ed.). 6-9 March 2000, Newport Beach, CA, United States, SPIE Digital Library, 2000. https://doi.org/10.1117/12.388847

[51]   Londoño, J. M.; Neild, S. A.; Wagg, D. J. Using a damper amplification factor to increase energy dissipation in structures. Engineering Structures, 2015, 84, pp.162-171. https://doi.org/10.1016/j.engstruct.2014.11.019

[52]   Spencer, B. F.; Sain, M. K. Controlling buildings: A new frontier in feedback [25 Years Ago]. IEEE Control Systems Magazine, 2022, 42 (6), pp. 12-13. https://doi.org/10.1109/mcs.2022.3209053

[53]   Dyke, S. J.; Spencer Jr., B. F.; Sain, M. K.; Carlson, J. D. An experimental study of MR dampers for seismic protection. Smart Materials and Structures,1998, 7 (5), pp. 693-703. https://doi.org/10.1088/0964-1726/7/5/012

[54]   Høgsberg, J.; Krenk, S. Energy dissipation control of magneto-rheological damper. Probabilistic Engineering Mechanics, 2008, 23 (2-3), pp.188-197. https://doi.org/10.1016/j.probengmech.2007.12.007

[55]   Shannag, M. J.; Abu-Dyya, N.; Abu-Farsakh, G. Lateral load response of high performance fiber reinforced concrete beam–column joints. Construction and Building Materials, 2005, 19 (7), pp. 500-508. https://doi.org/10.1016/j.conbuildmat.2005.01.007

[56]   Chidambaram, R. S.; Agarwal, P. Seismic behavior of hybrid fiber reinforced cementitious composite beam–column joints. Materials & Design, 2015, 86, pp.771-781. https://doi.org/10.1016/j.matdes.2015.07.164